Chapter 2

Discrete Methods

In this chapter, we review the procedures used in the classic discrete element method and contact dynamics to determine the contact forces and particle kinematics.

2.1 Discrete Element Method

The two defining features of the classic DEM [24] are particle deformability and the use of an explicit time integration algorithm to resolve particle collisions. Here, particle deformability refers to use of springs to model the contact forces, which act only when there is particle overlap. These two features imply that the time step must be smaller than the elastic response time for numerical stability. In this section, we discuss these two features in detail.

2.1.1 Normal force and associated moments

To show how the contact forces are calculated, we can focus on the case of single cohesionless contact between two particles. Consider a grain Ω^i with a potentially contacting neighbor grain Ω^j, as shown in Figure 2.1. The effective normal contact force on grain Ω^i at the contact point is calculated using a linear elastic stiffness model such that

$$\boldsymbol{f}_n^i = \begin{cases} k_N g\, \boldsymbol{n}, & \text{if } g < 0 \\ \boldsymbol{0}, & \text{otherwise} \end{cases} \tag{2.1}$$

where k_N is the normal elastic stiffness and $g\,\boldsymbol{n}$ measures the penetration or overlap in vector form, determined by some contact algorithm (e.g., the closest point projection operation

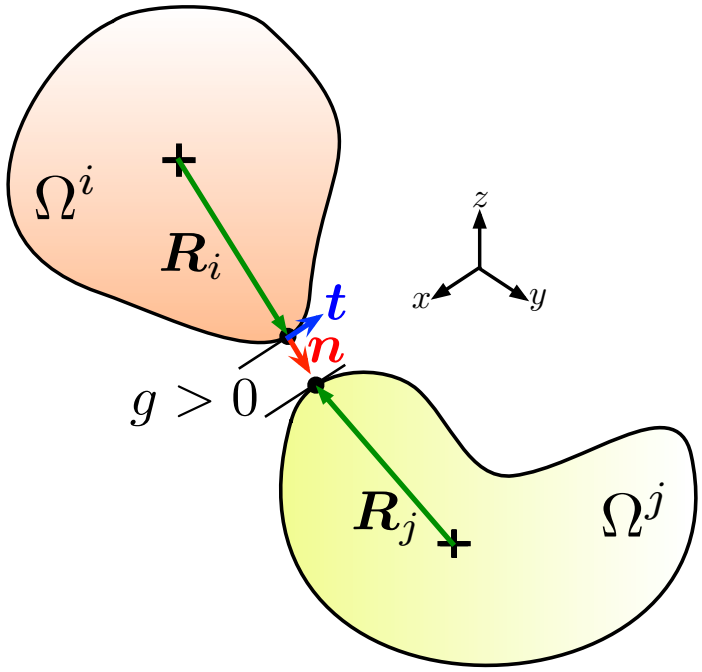

Figure 2.1: Illustration of two particles (Ω^i and Ω^j) that are potentially contacting. The gap g between the particles is positive if the particles are separated, and negative if the particles overlap. The moment arms emanating from each particle's centroid to its corresponding contact point are denoted by $\boldsymbol{R}_i$ and $\boldsymbol{R}_j$ for Ω^i and Ω^j, respectively.

described in Chapter 3). The sign convention used is that the normal vector $\boldsymbol{n}$ points away from the grain of interest, which means that $g\,\boldsymbol{n}$ with $g < 0$ has a direction pointing toward grain Ω^i. By action and reaction, the effective normal contact force on grain Ω^j contacting with grain Ω^i is then

$$\boldsymbol{f}_n^j = -\boldsymbol{f}_n^i \tag{2.2}$$

Denoting the moment arm extending from the centroid of grain Ω^i to the contact point by $\boldsymbol{R}_i$, the moment due to normal force is calculated as

$$\boldsymbol{m}_n^i = \boldsymbol{R}_i \times \boldsymbol{f}_n^i \tag{2.3}$$

Similarly, the moment due to normal force on the contacting grain Ω^j is

$$\boldsymbol{m}_n^j = \boldsymbol{R}_j \times \boldsymbol{f}_n^j \tag{2.4}$$

where $\boldsymbol{R}_j$ is the moment arm extending from the centroid of grain Ω^j to the contact point.

Remark 2.1.1 *In the case of disks or spheres, the signed gap g is calculated as*

$$g = R_i + R_j - \|\boldsymbol{x}_i - \boldsymbol{x}_j\| \tag{2.5}$$

where R_i and R_j are the radii of particles i and j, respectively. The corresponding particle centroids are $\boldsymbol{x}_i$ and $\boldsymbol{x}_j$.

2.1.2 Tangential force and associated moments

For simplicity, the incremental tangential forces are calculated here using the simple Coulomb friction model proposed in [24; 53]. In this model, the tangential stiffness is initialized at time of first contact and exists until the grains separate. The velocity of grain Ω^i relative to grain Ω^j at the contact point is calculated as

$$\boldsymbol{v}_{\text{rel}} = \boldsymbol{v}^i + \boldsymbol{\omega}^i \times \boldsymbol{R}_i - \boldsymbol{v}^j - \boldsymbol{\omega}^j \times \boldsymbol{R}_j \tag{2.6}$$

where $\boldsymbol{v}^i$ and $\boldsymbol{v}^j$ are the translational velocities, and $\boldsymbol{\omega}^i$ and $\boldsymbol{\omega}^j$ are the angular velocities in global coordinate frame of grains Ω^i and Ω^j, respectively. We then calculate the incremental displacement as

$$\Delta\boldsymbol{u} = \boldsymbol{v}_{\text{rel}}\Delta t \tag{2.7}$$

The increment in shear force on grain Ω^i is calculated as

$$\Delta\boldsymbol{f}_s^i = -k_T\Delta\boldsymbol{s} \tag{2.8}$$

where k_T is the shear spring stiffness and

$$\Delta\boldsymbol{s} = \Delta\boldsymbol{u} - (\Delta\boldsymbol{u}\cdot\boldsymbol{n})\,\boldsymbol{n} \tag{2.9}$$

is the tangential incremental displacement obtained by projecting the incremental displacement in the tangential direction. By action and reaction, the increment in shear force on grain Ω^j is

$$\Delta\boldsymbol{f}_t^j = -\Delta\boldsymbol{f}_t^i \tag{2.10}$$

Before the previous shear force can be updated, it needs to be corrected to account for the incremental rotation of the contact plane. The previous shear force vector at the contact point on grain Ω^p is first corrected as

$$\boldsymbol{f}_t^i := \boldsymbol{Z}\, \boldsymbol{f}_t^i \tag{2.11}$$

where $\boldsymbol{Z}$ is the rotation matrix that rotates the previous normal vector $\boldsymbol{n}^{\text{prev}}$ to the current normal vector $\boldsymbol{n}$. The shear force on grain Ω^i is updated as

$$\boldsymbol{f}_t^i := \boldsymbol{f}_t^i + \Delta \boldsymbol{f}_t^i \tag{2.12}$$

and then capped as

$$\boldsymbol{f}_t^i := \boldsymbol{f}_t^i \left(\frac{f_{\max}}{\|\boldsymbol{f}_t^i\|} \right) \tag{2.13}$$

where

$$f_{\max} = \|\boldsymbol{f}_n^i\| \tan \phi \tag{2.14}$$

with ϕ being the interparticle friction angle. Again, by action and reaction, the shear force on grain Ω^j contacting with grain Ω^j is

$$\boldsymbol{f}_t^j = -\boldsymbol{f}_t^i \tag{2.15}$$

Finally, the corresponding moments associated with the tangential forces are

$$\boldsymbol{m}_t^i = \boldsymbol{R}_i \times \boldsymbol{f}_t^i \tag{2.16}$$

$$\boldsymbol{m}_t^j = \boldsymbol{R}_j \times \boldsymbol{f}_t^j \tag{2.17}$$

for grains Ω^i and Ω^j, respectively.

2.1.3 Discrete equations of motion

In DEM, the equations of motion are integrated explicitly, particle-by-particle, using information from the previous time step. As such, in discussing the discrete equations of motion, we can focus on an individual particle. We assume that the resultant force and moment, obtained from summing all the forces and moments induced by contact interactions between

the particle and its contacting neighbors, are given. We first consider the translational components. The equation governing translational motion of the grain's center of mass is given by Newton's law:

$$M\,a_i + C\,v_i = F_i \tag{2.18}$$

where $i = 1, 2, 3$ in three dimensions, M is the mass of the grain, and $C = \xi M$ is the damping, which proportionally scales the linear velocity v_i, with ξ being the global damping parameter. The linear acceleration is given by a_i and is related to the resultant force F_i. To integrate the translational components of motion, we employ the centered finite-difference integration scheme proposed in [24]:

$$v_i^{n+1/2} = \frac{1}{1+\xi\Delta t/2}\left[(1-\xi\Delta t/2)\,v_i^{n-1/2} + \frac{\Delta t}{M}F_i\right] \tag{2.19}$$

$$x_i^{n+1} = x_i^n + \Delta t\,v_i^{n+1/2} \tag{2.20}$$

The control points of the NURBS patches in the grain are then translated by displacements according to $\Delta t\,v_i^{n+1/2}$.

For the 2D case, the discrete equations for integrating the rotational degree of freedom are analogous to those for the translations. For 3D, however, this is not the case. For the rotational components of motion in 3D, it is convenient to work in principal body-fixed frame. For the rest of this section, unless noted otherwise, we work with quantities that are defined with respect to the principal body-fixed frame. Consider the angular accelerations α_i given through the Euler's equations of motion as

$$\alpha_1 = \left[m_1 + \omega_2\,\omega_3(J_2 - J_3) - \xi J_1\,\omega_1\right]/J_1 \tag{2.21}$$

$$\alpha_2 = \left[m_2 + \omega_3\,\omega_1(J_3 - J_1) - \xi J_2\,\omega_2\right]/J_2 \tag{2.22}$$

$$\alpha_3 = \left[m_3 + \omega_1\,\omega_2(J_1 - J_2) - \xi J_3\,\omega_3\right]/J_3 \tag{2.23}$$

where ω_i for $i = 1, 2, 3$ are the angular velocities, m_i are the moments, and J_i are the principal moments of inertia. Here, inertia-proportional damping is included via the global damping parameter ξ. The Euler equations are nonlinear due to the presence of the products of angular velocities on the right hand side. Therefore, to appropriately integrate the

rotational components of motion, we use a predictor-corrector algorithm proposed in [54], which can be described in the following steps:

1. Estimate the angular velocities at the current time step by assuming constant angular acceleration for an additional half step:

$$\omega_i^{'n} = \omega_i^{n-\frac{1}{2}} + \frac{1}{2}\Delta\omega_i^{n-1} \tag{2.24}$$

   where $\Delta\omega_i^{n-1} = \alpha_i^{n-1}\Delta t$.

2. Calculate angular velocity predictors using the above estimates:

$$\Delta\omega_1^{'n} = \Delta t\left[m_1^n + \omega_2^{'n}\,\omega_3^{'n}(J_2 - J_3) - \xi J_1\,\omega_1^{'n}\right]/J_1 \tag{2.25}$$
$$\Delta\omega_2^{'n} = \Delta t\left[m_2^n + \omega_3^{'n}\,\omega_1^{'n}(J_3 - J_1) - \xi J_2\,\omega_2^{'n}\right]/J_2 \tag{2.26}$$
$$\Delta\omega_3^{'n} = \Delta t\left[m_3^n + \omega_1^{'n}\,\omega_2^{'n}(J_1 - J_2) - \xi J_3\,\omega_3^{'n}\right]/J_3 \tag{2.27}$$

3. Predict angular velocities at the current time step:

$$\omega_i^n = \omega_i^{n-\frac{1}{2}} + \frac{1}{2}\Delta\omega_i^{'n} \tag{2.28}$$

4. Calculate angular velocity correctors:

$$\Delta\omega_1^n = \Delta t\left[m_1^n + \omega_2^n\,\omega_3^n(J_2 - J_3) - \xi J_1\,\omega_1^n\right]/J_1 \tag{2.29}$$
$$\Delta\omega_2^n = \Delta t\left[m_2^n + \omega_3^n\,\omega_1^n(J_3 - J_1) - \xi J_2\,\omega_2^n\right]/J_2 \tag{2.30}$$
$$\Delta\omega_3^n = \Delta t\left[m_3^n + \omega_1^n\,\omega_2^n(J_1 - J_2) - \xi J_3\,\omega_3^n\right]/J_3 \tag{2.31}$$

   Additional iterations are performed by repeating steps 1 through 4 until the correctors converge to some desired tolerance.

5. Update angular velocities using the correctors:

$$\omega_i^{n+\frac{1}{2}} = \omega_i^{n-\frac{1}{2}} + \Delta\omega_i^n \tag{2.32}$$

For small time steps used to resolve the interparticle contacts and for quasi-static conditions

in which the angular velocities are small, the number of iterations is typically small. Usually, between 3 and 5 iterations are required to achieve machine precision tolerance.

After obtaining the angular velocities, the orientation of the principal body-fixed frame is updated using the singularity-free quaternion approach in [55], which is described as follows. The rotation matrix that transforms vectors in global space to vectors in body frame is given by

$$\mathbf{A} = \begin{pmatrix} -q_1^2 + q_2^2 - q_3^2 + q_4^2 & -2\,(q_1\,q_2 - q_3\,q_4) & 2\,(q_2\,q_3 + q_1\,q_4) \\ -2\,(q_1\,q_2 + q_3\,q_4) & q_1^2 - q_2^2 - q_3^2 + q_4^2 & -2\,(q_1\,q_3 - q_2\,q_4) \\ 2\,(q_2\,q_3 - q_1\,q_4) & -2\,(q_1\,q_3 + q_2\,q_4) & -q_1^2 - q_2^2 + q_3^2 + q_4^2 \end{pmatrix} \tag{2.33}$$

where the q_i's are the quaternions defined by

$$q_1 = \sin\left(\frac{\theta}{2}\right) \sin\left(\frac{\psi - \phi}{2}\right) \tag{2.34}$$

$$q_2 = \sin\left(\frac{\theta}{2}\right) \cos\left(\frac{\psi - \phi}{2}\right) \tag{2.35}$$

$$q_3 = \cos\left(\frac{\theta}{2}\right) \sin\left(\frac{\psi + \phi}{2}\right) \tag{2.36}$$

$$q_4 = \cos\left(\frac{\theta}{2}\right) \cos\left(\frac{\psi + \phi}{2}\right) \tag{2.37}$$

and ϕ, θ, and ψ are the Euler angles in the $z\,x'z'$ notational convention [56]. The initial values of the quaternions are calculated using the initial configurations of the grains before the start of the simulation.

The time derivatives of the quaternions can be expressed in terms of products of the quaternions with the angular velocities as a singularity-free set of equations:

$$\begin{pmatrix} \dot{q}_1 \\ \dot{q}_2 \\ \dot{q}_3 \\ \dot{q}_4 \end{pmatrix} = \frac{1}{2} \begin{pmatrix} -q_3 & -q_4 & q_2 \\ q_4 & -q_3 & -q_1 \\ q_1 & q_2 & q_4 \\ -q_2 & q_1 & -q_3 \end{pmatrix} \begin{pmatrix} \omega_1 \\ \omega_2 \\ \omega_3 \end{pmatrix} \tag{2.38}$$

with closure of the above system given by the normalization relation

$$\sum_{i=1}^{4} q_i = 1 \tag{2.39}$$

The above system of equations can be solved using an explicit finite difference scheme [54], which results in the following update equation:

$$\mathbf{q}^{n+1} = \mathbf{B}^{-1}\mathbf{B}^{T}\mathbf{q}^{n} \tag{2.40}$$

where

$$\mathbf{q}^{n} = \begin{pmatrix} q_1^n \\ q_2^n \\ q_3^n \\ q_4^n \end{pmatrix}, \quad \mathbf{B} = \begin{pmatrix} 1 & -\beta_3 & \beta_1 & \beta_2 \\ \beta_3 & 1 & \beta_2 & -\beta_1 \\ -\beta_1 & -\beta_2 & 1 & -\beta_3 \\ -\beta_2 & \beta_1 & \beta_3 & 1 \end{pmatrix} \tag{2.41}$$

and

$$\beta_i = \frac{\Delta t}{4}\omega_i^{n+\frac{1}{2}} \tag{2.42}$$

and where $\square^T$ is the transpose operator. We note that equation (2.40) can be solved in closed form as described in [54]. It has been shown in [55] that equation (2.38) maintains the orthogonality relation of equation (2.39). Normalization of the quarternions, however, is performed after each integration step to prevent normalization failure resulting from round-off error.

The matrix $\mathbf{A}^{n+1}$ of equation (2.33) at t_{n+1} can be evaluated using the quaternions in $\mathbf{q}^{n+1}$. The updated orientation (triads) of the principal body-fixed frame is then given by the rows $\mathbf{A}^{n+1}$. The required rotation matrix for rotating the particle about its center of mass is obtained as

$$\mathbf{\Pi}^{n+1} = \mathbf{A}^{n+1\,T}\mathbf{A}^{n} \tag{2.43}$$

In the next calculation cycle, the moments on each grain due to interparticle contact, calculated in the global frame, are transformed into the principal body-fixed frame using $\mathbf{A}^{n+1}$.

Damping is used to achieve quasi-static conditions by utilizing the so-called dynamic relaxation, which allows the dissipation of accelerations, hence making all resulting forces

vanish, achieving in this way static equilibrium [57].

Verification tests on the classic DEM are shown in Appendix A.1.

2.2 Contact Dynamics

In contrast with DEM, CD considers the deformation of the granular medium as a whole, determined exclusively by geometric rearrangements of rigid particles [58]. The CD formulation appears to originate from the works of Lötstedt [59; 60], which provide the formulation of the contact problem between rigid bodies as a linear complementarity problem (LCP). Further analysis and development of solution procedures by Moreau [61] and Jean [62] led to the introduction of CD to the granular materials research community.

In this section, we provide the basics of CD and highlight the major differences between CD and DEM. For simplicity, we will work under the assumption of near quasi-static conditions in which the angular velocities are small. In this case, the terms containing products of angular velocities in equation (2.23) are neglected. In addition, for the purpose of illustrating the time integration scheme, we will assume that the coefficient of restitution between two particles is zero. This assumption can be shown to correspond to the fully implicit or backward Euler scheme (see Chapter 4).

The rigidity of the particles requires that the non-penetration constraint is enforced between particles. This constraint is embodied in the non-smooth graph of normal reaction force versus the gap or separation between two particles, as shown in Figure 2.2(a). The non-

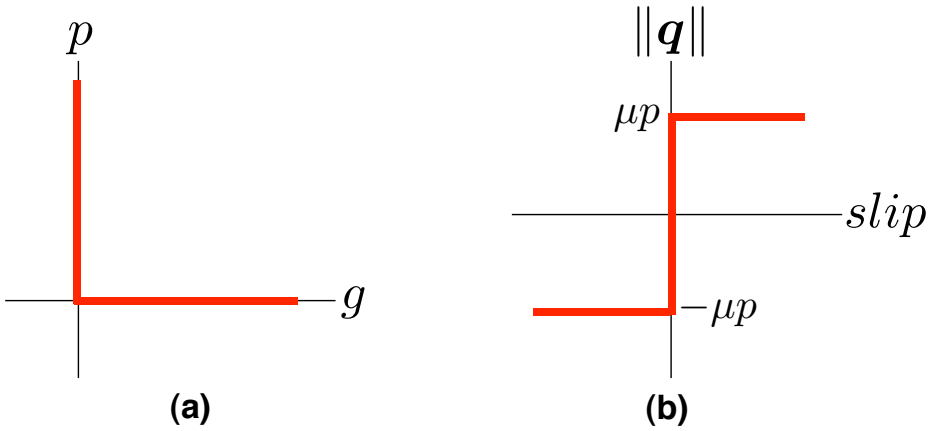

Figure 2.2: Graph of non-smooth contact laws: (a) normal reaction force p against separation or gap g and (b) friction force $\|\boldsymbol{q}\|$ against slip; μ is the friction coefficient.

penetration constraint is sometimes described as unilateral, which means that the normal reaction is active when the gap is zero and is zero otherwise. In addition, a non-sliding constraint of frictional contacts is required. The most basic of such constraint is given by the Coulomb threshold, as shown in Figure 2.2(b).

To explain the single-contact update procedure, consider the following generalized velocity and force vectors:

$$\boldsymbol{V} = \begin{pmatrix} \boldsymbol{v}^i \\ \boldsymbol{\omega}^i \\ \boldsymbol{v}^j \\ \boldsymbol{\omega}^j \end{pmatrix} \tag{2.44}$$

$$\boldsymbol{\Lambda} = \begin{pmatrix} \boldsymbol{\lambda} \\ \boldsymbol{R}_i \times \boldsymbol{\lambda} \\ -\boldsymbol{\lambda} \\ -\boldsymbol{R}_j \times \boldsymbol{\lambda} \end{pmatrix} \tag{2.45}$$

where $\boldsymbol{\lambda}$ is the yet to be determined constraint force, and $\boldsymbol{R}_i, \boldsymbol{R}_j$ are again the moment arms, as shown in Figure 2.1. We can reexpress equations (2.45) in linear form as

$$\boldsymbol{\Lambda} = \begin{pmatrix} \mathbf{I} \\ -\mathbf{R}_i \\ -\mathbf{I} \\ \mathbf{R}_j \end{pmatrix} \boldsymbol{\lambda} = \boldsymbol{H}\boldsymbol{\lambda} \tag{2.46}$$

where $\mathbf{R}_i$ is the matrix containing the components of the radius vector $\boldsymbol{R}_i$ arranged in the form

$$\mathbf{R}_i = \begin{bmatrix} 0 & -R_{i,3} & R_{i,2} \\ R_{i,3} & 0 & -R_{i,1} \\ -R_{i,2} & R_{i,1} & 0 \end{bmatrix} \tag{2.47}$$

The relative velocity (2.6) can then be written as

$$\boldsymbol{v}_{\text{rel}} = \boldsymbol{H}^T \boldsymbol{V} \tag{2.48}$$

The equations of motion for the two interacting particles are given by

$$\frac{d\boldsymbol{V}}{dt} = \boldsymbol{M}_{\text{eff}}^{-1} \left(\boldsymbol{\Lambda} + \boldsymbol{F}_{\text{ext}} \right) \tag{2.49}$$

where $\boldsymbol{M}_{\text{eff}}$ is the effective mass matrix given by

$$\boldsymbol{M}_{\text{eff}} = \begin{bmatrix} m^i \mathbf{1} & 0 & 0 & 0 \\ 0 & J^i \mathbf{1} & 0 & 0 \\ 0 & 0 & m^j \mathbf{1} & 0 \\ 0 & 0 & 0 & J^j \mathbf{1} \end{bmatrix} \tag{2.50}$$

and $\boldsymbol{F}_{\text{ext}}$ is the generalized external load vector containing the external translational forces and moments acting on the particles. Using equations (2.46) and (2.48), we can rewrite (2.49) as

$$\frac{d\boldsymbol{v}_{\text{rel}}}{dt} = \boldsymbol{H}^T \boldsymbol{M}_{\text{eff}}^{-1} \boldsymbol{H} \boldsymbol{\lambda} + \frac{d\boldsymbol{v}_{\text{free}}}{dt} \tag{2.51}$$

where

$$\frac{d\boldsymbol{v}_{\text{free}}}{dt} = \boldsymbol{H}^T \boldsymbol{M}^{-1} \boldsymbol{F}_{\text{ext}} \tag{2.52}$$

is the acceleration without any interaction between the particles.

Discretizing equation (2.51) using a backward Euler scheme gives the discrete equation corresponding to equation (2.51) as

$$\frac{\boldsymbol{v}_{\text{rel}} - \boldsymbol{v}_{\text{free}}}{\Delta t} = \boldsymbol{H}^T \boldsymbol{M}_{\text{eff}}^{-1} \boldsymbol{H} \boldsymbol{\lambda} \tag{2.53}$$

with the new velocity without any interaction between the particles calculated as

$$\boldsymbol{v}_{\text{free}} = \boldsymbol{v}_{\text{rel}}^0 + \boldsymbol{H}^T \boldsymbol{M}^{-1} \boldsymbol{F}_{\text{ext}} \Delta t \tag{2.54}$$

where the quantities $\boldsymbol{\lambda}$ and $\boldsymbol{v}_{\text{rel}}$ are unknowns and $\boldsymbol{v}^0_{\text{rel}}$ is the known relative velocity from the previous time step. To determine the unknowns, the steps in Algorithm 1 are applied.

1: Check if gap is open after one time step: $g + \Delta t\, \boldsymbol{v}_{\text{free}} \cdot \boldsymbol{n} > 0$? Yes, set $\boldsymbol{\lambda} = \boldsymbol{0}$ and $\boldsymbol{v}_{\text{rel}} = \boldsymbol{v}_{\text{free}}$ and exit. No, go to next step.

2: Compute new relative velocity assuming gap is closed: $g + \Delta t\, \boldsymbol{v}_{\text{rel}} \cdot \boldsymbol{n} = 0$. Assume non-sliding contact, i.e., zero tangential velocity $\boldsymbol{v}_{t\,\text{rel}} = \boldsymbol{0}$. Let $\boldsymbol{v}_{\text{rel}} = -(g/\Delta t)\boldsymbol{n}$. Compute:

- Constraint force $\boldsymbol{\lambda}$ from equation (2.53)
- Contact normal force $p = \boldsymbol{\lambda} \cdot \boldsymbol{n}$
- Contact shear force $\boldsymbol{q} = \boldsymbol{\lambda} - p\boldsymbol{n}$

Check Coulomb threshold: $\|\boldsymbol{q}\| \leq \mu p$? Yes, accept $\boldsymbol{v}_{\text{rel}}$, $\boldsymbol{\lambda}$ and exit. No, go to next step.

3: Gap is still closed $f = 0$ but $\boldsymbol{v}_{t\,\text{rel}} \neq \boldsymbol{0}$. Let $\boldsymbol{v}_{\text{rel}} = -(g/\Delta t)\boldsymbol{n} + \boldsymbol{v}_{t\,\text{rel}}$. Solve equation (2.53) for $\boldsymbol{\lambda}$ and $\boldsymbol{v}_{t\,\text{rel}}$ subject to:

$$\boldsymbol{q} = -\mu\, p\, \frac{\boldsymbol{v}_{t\,\text{rel}}}{\|\boldsymbol{v}_{t\,\text{rel}}\|}$$

Algorithm 1: Single-Contact Update Algorithm

Remark 2.2.1 *Algorithm 1 is reminiscent of the return mapping algorithm used for elasto-plasticity constitutive updates [63].*

We note that Algorithm 1 applies only to the single-contact case. In general, the multi-contact case applies, in which case the generalized load vector includes constraint forces and moments from neighboring contacts. It can then be shown that the resulting global equilibrium equation resembles a Laplace-type equation that couples all the constraint forces and moments, and hence these cannot be computed locally. Moreover, these constraint forces need to satisfy the non-penetration and non-sliding constraints at every contact. An iterative scheme is applied within each time step to obtain a globally consistent set of forces satisfying all the required constraints. In each iteration, a contact is selected and updated based on the contact law for the single-contact case, independent of the other contacts. The selection of contact for update is performed randomly through either a sweep or sequentially over the contact set. In the case of a random sweep, each contact is selected exactly once within the iteration while for the random sequential update, the same contact could be selected more than once. The iterative procedure causes a relaxation of forces to a globally consistent solution analogous to the behavior of information spreading in a diffusive (heat)

system. For a system with rigid particles, the number of unknowns in general exceeds the number of equilibrium equations. As such, there could be more than one globally consistent solution to the system. Therefore, it is crucial that the selection of contacts avoids any bias in information spreading in the system during the relaxation process.

Alternatively, the coupling of all the constraint forces and moments can be dealt with by directly solving the mixed LCP associated with the discrete update equations and contact constraints [64–68]. While small instances of LCPs often can be solved efficiently by means of pivot based algorithms such as that of Lemke [69], methods for larger problems still lag far behind current convex program solvers [70], e.g., second-order cone programs (SOCPs), as far as efficiency and robustness are concerned. Newton-based algorithms for LCP have also been developed [71] and although these methods in principle offer the same advantages as their convex programming counterparts, their performance has been shown to be highly problem dependent and convergence is generally not guaranteed. Moreover, while convex programs admit a straightforward analysis of existence and uniqueness properties (and most implementations automatically detect infeasibility, i.e., non-existence), LCPs are in general much harder to gauge with respect to these properties. This leads to a situation where one is unable to distinguish between algorithmic failure and non-existence of solutions [72].

In general, the implementation of solution procedures for CD is quite complicated and this remains the primary reason why CD has not been widely adopted by the granular research community despite favorable performance that has been shown through a number of studies [73–83]. In Chapter 4, we present a new formulation of CD that is numerically more palatable and significantly easier to implement.